Journal of Alloys and Compounds 724 (2017) 67–73

Contents lists available at ScienceDirect

Journal of Alloys and Compounds

journal homepage: http://www.elsevier.com/locate/jalcom

Magnetic properties, x-ray absorption spectroscopy and electronic structure of $GdCrTiO_5$

E.B. Guedes [a, *], H.P. Martins [a], M. Abbate [a], S.H. Masunaga [b], F.E.N. Ramirez [b], R.F. Jardim [b], R.J.O. Mossanek [a]

[a] Departamento de Física, Universidade Federal do Paraná, Caixa Postal 19044, 81531-990, Curitiba, PR, Brazil
[b] Instituto de Física, Universidade de São Paulo, Rua do Matão, 1371, CEP 05508-090, São Paulo, SP, Brazil

ARTICLE INFO

Article history:
Received 6 April 2017
Received in revised form
29 June 2017
Accepted 30 June 2017
Available online 3 July 2017

Keywords:
$GdCrTiO_5$
Magnetic susceptibility
X-ray absorption
Density Functional Theory

ABSTRACT

We study the electronic structure of $GdCrTiO_5$ polycrystals by means of magnetic susceptibility and heat capacity measurements, as well as x-ray absorption spectroscopies on the Cr 2*p*, Ti 2*p* and O 1*s* levels. The experimental results were interpreted with Charge Transfer Multiplet and Density Functional Theory calculations. Magnetic susceptibility and specific heat measurements indicate a long-range antiferromagnetic ordering at 0.9 K probably related to the Gd sublattice. The results indicate that spin-orbit interaction, rather than hybridization, may be crucial for the stabilization of magnetic ordering in the $RCrTiO_5$ (R = rare earth) family.

1. Introduction

The coupling between ferromagnetism and ferroelectricity was first conceived by Pierre Curie and has attracted a great deal of attention since then [1]. Early works focused mainly on the mechanism of the magnetoelectric (ME) effect, particularly of Cr_2O_3 [2–5]. Attention to this class of materials was reinforced due to the observation of large responses to applied fields in multiferroic compounds [6–9]. The interest lies not only in the new physics, but also in possible applications in memory devices and spintronics [10]. Relatively well-known examples include the RMn_2O_5 family (R = Y, Tb, Pr, Eu, Dy, and others) [11–14].

The $RCrTiO_5$ family have also received attention due to the controversy regarding the R = Nd member. The $NdCrTiO_5$ compound crystallizes in a mullite-like structure with orthorhombic unit cell and space group *Pbam* [15]. The Cr^{3+} ions occupy the center of distorted octahedra of O^{2-} ions (O_h symmetry), which share corners with the O^{2-} pyramids that surround the Ti^{4+} ions (C_{4v} symmetry), whereas the Nd^{3+} ions occupy the interstitial regions [15]. Neutron diffraction studies revealed the presence of two distinct magnetic sublattices below the antiferromagnetic transition temperature [16]. It has been suggested that the Cr^{3+} sublattice is coupled to the Nd^{3+} sublattice by means of Cr 3*d*–Nd 4*f* hybridization [7,17]. The study on the electrical properties revealed characteristics in the dielectric constant and the pyroelectric current which would favor a scenario based on the linear ME effect, rather than ferroelectricity [18]. Saha et al. [15] argued that $NdCrTiO_5$ is a genuine multiferroic material possibly driven by non-collinear magneto-striction. Magnetic and electric measurements on $Nd_{1-x}Eu_xCrTiO_5$, $NdCr_{1-y}Al_yTiO_5$ [7] and $Nd_{1-x}Sm_xCrTiO_5$ [17] indicated that Eu, Al and Sm substitutions are detrimental to the magnetic ordering, and that Nd 4*f*–Cr 3*d* hybridization may play an important role in determining the non-collinear magnetic ground state reported in $NdCrTiO_5$.

The $GdCrTiO_5$ compound (R = Gd), which has the same crystal structure as $NdCrTiO_5$, is another member of the $RCrTiO_5$ family that has been studied over the last years. Indeed, the magnetic and electric properties of this compound were recently reported [19]. The authors observed the existence of magnetodielectric coupling and short-range magnetic order in this system, although no signal of long-range magnetic order is observed down to 2 K. This result is

* Corresponding author.
E-mail address: eboniniguedes@gmail.com (E.B. Guedes).

http://dx.doi.org/10.1016/j.jallcom.2017.06.335
0925-8388/

interesting because the R = Nd counterpart orders antiferromagnetically around 21 K, even though Gd^{3+} ($4f^7$) carries a higher magnetic moment than Nd^{3+} ($4f^3$). This lead the authors to attribute the lack of ordering of the Cr^{3+} network to a weak Gd 4*f*–Cr 3*d* hybridization, caused by a reduced radial extension of the Gd 4*f* orbitals in comparison to Nd 4*f* orbitals.

The possible existence of another mechanism instead of 4*f*–3*d* hybridization causing the noncollinear antiferromagnetic state in this family has not been discussed in the literature. For 3*d* transition-metal ions, the orbital moment of the *d* shells is usually considered quenched ($L = 0$), in which cases the spin-orbit interaction is weaker than the crystal field interaction. In turn, the spin-orbit interaction may become relevant in *f* shells, specially for ions with high atomic number Z, which is the case for Nd and Gd, because it is proportional to Z^4. Jang et al. [20] recently demonstrated that even in half-filled electron systems, the orbital angular moment can be an important parameter to describe material properties, and may provide significant opportunities for tailoring new correlated electron systems.

With this in mind, we have performed a comprehensive study of $GdCrTiO_5$ polycrystals by means of magnetic susceptibility and heat capacity measurements, as well as x-ray absorption spectroscopy on the Cr 2*p*, Ti 2*p* and O 1*s* levels. The experimental results were interpreted with Charge Transfer Multiplet (CTM) and Density Functional Theory (DFT) calculations. The behavior of magnetic susceptibility, specially below 2 K, and effective magnetic moment were also studied. Our findings point to the fact that the spin-orbit interaction, instead of hybridization, should play an important role in stabilizing the two non-collinear magnetic sublattices in the $RCrTiO_5$ family.

2. Experimental details

Polycrystalline samples of $GdCrTiO_5$ were prepared by mixing and grinding appropriate amounts of Gd_2O_3, Cr_2O_3, and TiO_2, followed by a heat treatment performed at 1000 °C for 24 h. The specimens were reground, pelletized, and sintered in air at 1300 °C for 50 h, a step that has been repeated three times. The X-ray powder diffraction (XRD) pattern was collected on a Brucker D-8 Discovery diffractometer equipped with a Cu K_α radiation in the 2θ range 10°–120°, with a step size of 0.02° at room temperature.

Measurements of dc and ac magnetic susceptibility were performed in the powder samples by using a superconducting quantum interference device magnetometer (SQUID) from Quantum Design. The dc curves were taken under zero-field-cooled (ZFC) and field-cooled (FC) processes, in several applied magnetic fields ($50 \leq H \leq 70000$ Oe), and in the temperature range of 2–300 K. A magnetic susceptibility curve down to 0.6 K and under 5 kOe was also obtained using a vibrating sample magnetometer (VSM) in a He^3 refrigerator. On the other hand, ac magnetic susceptibility curves were performed at 1 Hz with an oscillating field of 1 Oe under various applied magnetic fields (up to 30 kOe). Heat capacity measurements were performed using the thermal-relaxation technique in a Quantum Design Physical Property Measurement System (PPMS), in the 0.05–20 K temperature range.

The Cr 2*p*, Ti 2*p* and O 1*s* levels x-ray absorption spectra were measured at the PGM beamline, at the Laboratório Nacional de Luz Síncrotron (LNLS), Brazil. The energy resolution was set to approximately 0.5 eV. The photon energy scale was calibrated using the peak position of reference samples. The pressure in the experimental chamber was about 1×10^{-9} mbar. All the spectra were acquired at room temperature using the total electron yield mode. The sample was scraped with a diamond file to remove surface contamination.

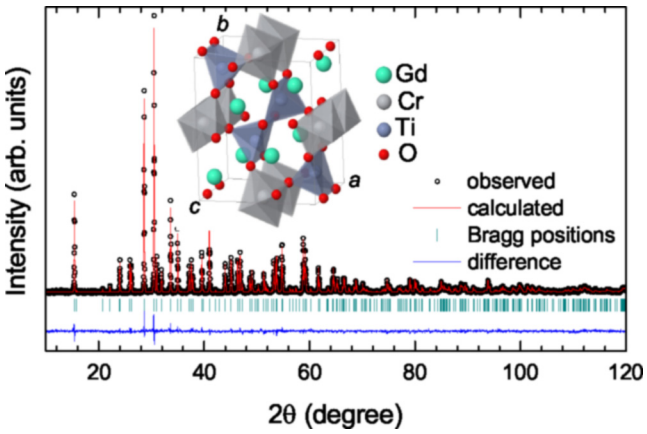

Fig. 1. X-ray diffraction pattern for the $GdCrTiO_5$ sample (symbols) taken at room temperature, calculated pattern (red line), their difference (blue line), and Bragg positions (ticks). The inset displays the crystal structure of the $GdCrTiO_5$ compound. (For interpretation of the references to colour in this figure legend, the reader is referred to the web version of this article.)

3. Calculation details

3.1. Charge transfer multiplet calculations

The Cr 2*p* and Ti 2*p* x-ray absorption spectra were simulated using multiplet calculations including ligand field effects [21]. The results were projected in the appropriate crystal field symmetry for each metal ion. The crystal field parameters 10Dq, which controls the splitting of the *d* levels in octahedral symmetry, as well as Dt and Ds, responsible for further splitting the levels in square-planar symmetry [22], were adjusted to provide the best agreement with the measurements. The Slater integrals were reduced to 80% of their original values to account for intra-atomic screening.

The charge transfer effects are included by expanding the initial and final states using the configuration interaction method. The initial state $2p^6\ 3d^n$ is expanded beyond the ionic approximation to include charge transfer configurations such as $2p^6\ 3d^{n+1}\underline{L}$ and $2p^6\ 3d^{n+2}\underline{L}^2$ (where $\underline{L}$ denotes an O 2*p* hole). This same treatment is made for the final states. The model parameters used in the charge transfer calculations are: the charge transfer energy Δ, the Mott-Hubbard repulsion U, and the M 3*d*–O 2*p* hybridization T_σ [23]. The M 2*p* core-hole potential is included via a Q = U/0.83 parameter [23]. The initial set of parameters for both metal ions were first obtained from interpolation of the available data [24].

The calculated spectra were broadened with Gaussian functions to simulate the experimental resolution, and with Lorentzian functions to account for the finite lifetime of the corresponding core hole. The FWHM values for the Lorentzian broadening widths were taken from reference tables [25]. The spectra were rigidly shifted to have a better match with the energy positions of the structures in the experiment.

3.2. Band structure calculations

The band structure calculations were performed with the full-potential linearized augmented plane-wave + local orbitals method, implemented in the WIEN2k package [26]. The experimental orthorhombic lattice parameters were used. Non-magnetic (N), ferromagnetic (FM) and antiferromagnetic (AFM) solutions were admitted. For the AFM calculation, the unit cell was split into two magnetic sublattices and oriented antiferromagnetically as in Kori et al. [7], but with a collinear alignment along the *c* axis. The calculations were carried within the generalized gradient

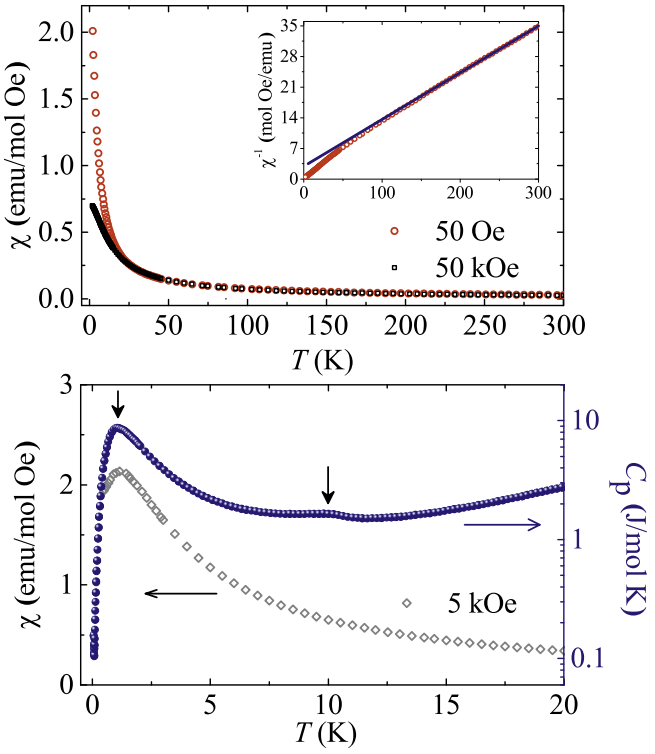

Fig. 2. (Top) dc Magnetic susceptibility curves (χ) measured at $H = 50$ Oe and 50 kOe. The inset shows the temperature dependence of the inverse dc susceptibility $\chi^{-1}(T)$ for $H = 50$ Oe. The blue line serves as guide to the eye. (bottom) The expanded view of $\chi(T)$ for $H = 5$ kOe and $C_p(T)$ in the low temperature region. The arrows indicate the position of two transition temperatures: T_{N1} and T_{N2}. (For interpretation of the references to colour in this figure legend, the reader is referred to the web version of this article.)

approximation (PBEsol functional) [27]. The k-mesh was set to a $6 \times 5 \times 8$ grid, and the convergence criteria for the energy was 10^{-6} eV. To understand the possible role of the Gd 4*f* spin-orbit (SO) interaction in this compound, the calculations were done with and without this effect.

4. Results and discussion

4.1. X-ray diffraction and magnetization analysis

The XRD pattern of the $GdCrTiO_5$ sample along with the Rietveld refinement using the GSAS [28] program are displayed in Fig. 1. The values of goodness-of-fit and weighted-profile reliability obtained from the refinement were $\chi^2 = 1.8$ and $R_{wp} = 2.5\%$, respectively. We can see that the sample is single-phase, belonging to orthorhombic space group *Pbam*(55). The unit cell parameters found from Rietveld refinement are $a = 7.4365(3)$ Å, $b = 8.5851(4)$ Å, and $c = 5.7806(3)$ Å, which are in excellent agreement with a previous report [16], and in contrast to the parameter *b* recently reported [19].

Top panel of Fig. 2 shows dc magnetic susceptibility $\chi(T)$ curves measured from 2 to 300 K in two magnetic fields. The ZFC and FC curves converge in the temperature range measured, indicating a typical paramagnetic behavior. At low temperatures, the magnitude of χ decreases abruptly when the external magnetic field is increased. The temperature dependence of the inverse dc susceptibility (χ^{-1}) for $H = 50$ Oe is depicted in the inset of Fig. 2. The curve $\chi^{-1}(T)$ exhibits a linear behavior for temperatures above $= 100\,K$, indicating the existence of magnetic exchange interactions below this temperature. The expected spin-only magnetic moment for the bulk compound may be calculated by using the equation for non-collinear moments $\mu^2_{eff} = \mu^2_{eff(Gd)} + \mu^2_{eff(Cr)}$, where $\mu_{Cr} = 3.87\mu_B$ and $\mu_{Gd} = 7.94\mu_B$, resulting $8.83\mu_B$. The effective magnetic moment and Curie-Weiss temperature (θ_{CW}), obtained from the linear fitting, were $8.83\mu_B$ and −33 K, respectively. Thus, our experimental μ_{eff} value agrees well with the expected one and the negative sign of θ_{CW} indicates dominant antiferromagnetic exchange interactions in the system. In order to get a better insight into the magnetic behavior of our sample, dc magnetic susceptibility and heat capacity $C_p(T)$ measurements were conducted at temperatures down to 0.6 K. The results, displayed in the bottom panel of Fig. 2, exhibit a well-defined anomaly at $T_{N1} = 0.9$ K in both $\chi(T)$ and $C_p(T)$ curves, suggesting the occurrence of long-range magnetic ordering associated with the Gd sublattice, a feature not observed in a previous report [19]. Another feature at $T_{N2} \sim 10$ K is only observed in the $C_p(T)$ data.

The temperature dependence of real part of ac magnetic susceptibility ($\chi'(T)$) measured at several characteristic frequencies with $H_{ac} = 1$ Oe and $H_{dc} = 20$ kOe is displayed in the top panel of Fig. 3. We first mention that the magnetic behavior of $\chi'(T)$ is complex and certainly related to the two magnetic sublattices (Cr and Gd) of the system. It shows a strong frequency dependence of $\chi'(T)$, a feature much more pronounced at low frequencies. For $f =$ 0.3 Hz, a broad peak around $T_{max} = 11.5$ K, which compares well with C_p results, is observed. With increasing frequency, up to 3 Hz, the peak becomes rounded, shorter, and shifts to higher

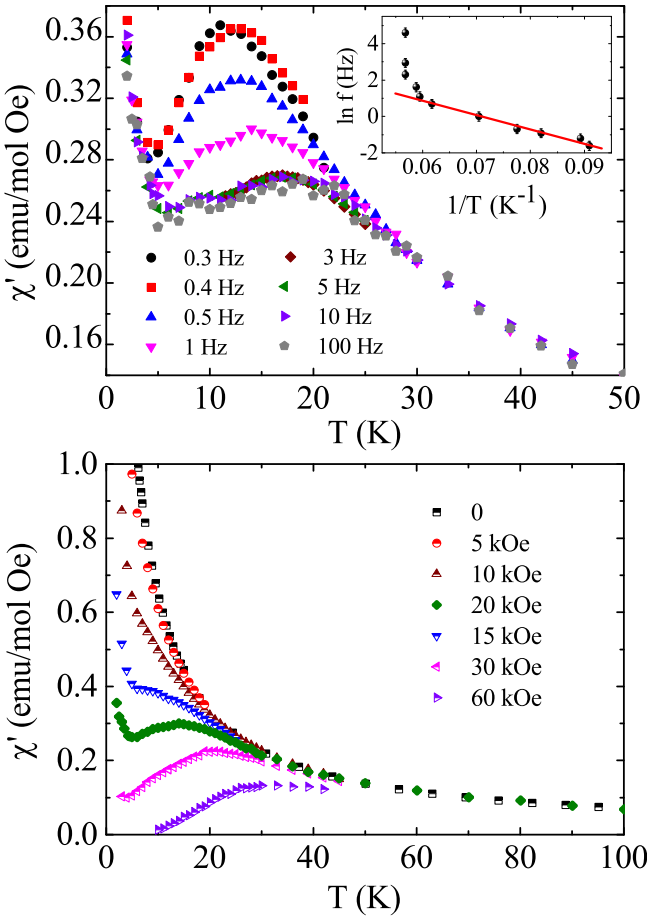

Fig. 3. Temperature dependence of the real part of ac magnetic susceptibility measured at $H_{ac} = 1$ Oe at several (top) characteristic frequencies and (bottom) external dc magnetic fields.

temperatures. The shape and the peak temperature observed in the χ' component is no longer affected by further increase in f up to 100 Hz. For $f < 3$ Hz, a careful analysis indicated that the variation the peak position with frequency does not follow the relationship $f = f_0[T_f/(T_{max}-T_f)]^{\beta}$, where f_0 is the effective attempt frequency and T_f is the freezing temperature, commonly seen in system with spin glass behavior. This result along with the lack of difference between field-cooled and zero-field-cooled dc magnetic susceptibility curves discard the existence of a spin-glass state in $GdCrTiO_5$. We have also investigated the shift of the peak in $\chi'(T)$ by using the Arrhenius law $f = f_0 \exp(E_a/k_BT)$, where E_a is the energy barrier to spin relaxation, in the frequency range between 0.3 and 3 Hz (see inset of Fig. 3). From the fitting procedure, we have found an unusual small value for $f_0 = 284$ Hz whereas E_a was 79 K, respectively.

Focusing on the low-frequency behavior of ac magnetic susceptibility in $GdCrTiO_5$, the bottom panel of Fig. 3 displays $\chi'(T)$ curves measured under several magnetic fields at $f = 1$ Hz and $H_{ac} = 1$ Oe. For $H < 15$ kOe, χ' exhibits a similar behavior when compared to the dc magnetic susceptibility data, i.e., the compound behaves as a paramagnetic material. However, for $H > 15$ kOe, a weak and broad maximum, reminiscent of the feature observed in $C_p(T)$ data, appears at temperatures close to 11 K. The temperature of the maximum is shifted towards higher temperatures with increasing external magnetic field: for example, it is 13.8, 20.8, and 32 K for $H = 20$, 30 kOe, and 60 kOe, respectively. These results suggest the existence of short-range magnetic correlations which are induced by the application of an external dc magnetic field and probably related to very slow spin relaxation processes.

Basu et al. [19] have suggested that $3d-4f$ hybridization in the $GdCrTiO_5$ compound is small because the $4f$-radial extension decreases as one moves away from Nd and towards heavier rare-earths. The authors also observed the existence of one anomaly around 10 K, which was attributed to magnetic ordering of Cr sublattice. On the contrary, our work suggests (See section 4.4) that it is possible to assume that the Gd and Cr magnetic sub-lattices are not coupled through hybridization. Thus, the anomalies at T_{N1} and T_{N2} could be attributed to antiferromagnetic transition from Gd sublattice and short-range antiferromagnetic ordering of Cr ions, respectively. Note that the transition temperatures T_{N1} and T_{N2} are much less than those observed in the $NdCrTiO_5$ counterpart, and this feature will also be addressed below.

4.2. Cr 2p and Ti 2p x-ray absorption

Fig. 4 presents the comparison between the experimental x-ray absorption spectra and the covalent multiplet calculations. The spectrum reflects transitions from occupied Cr/Ti $2p_{3/2}$ and $2p_{1/2}$ levels to unoccupied $3d$ levels. Both spectra are split into the $2p_{3/2}$ and $2p_{1/2}$ parts, as indicated in the figure.

The calculations were performed in an octahedral crystal field symmetry (O_h) for Cr^{3+} and in a square planar symmetry (C_{4v}) for the Ti^{4+} ions. The crystal field parameters 10Dq, Dt and Ds used in the calculations can be seen in Table 1, along with the charge transfer energy Δ, the Mott-Hubbard repulsion U, and the M $3d$–O $2p$ hybridization T_σ (all values in eV) [21,22].

The top panel of Fig. 4 presents the results for Cr^{3+}. The $2p_{3/2}$ part of the experimental spectrum is composed of a shoulder around 575.5 eV, a small peak around 576.5 eV, the major peak around 577.5 eV and a set of shoulders centered at 579 eV. The $2p_{1/2}$ region presents the same overall shape, but with reduced intensity and less features due to the increase of the lifetime broadening. The bottom panel of Fig. 4 presents the results for Ti^{4+}. The $2p_{3/2}$ region of the spectrum is composed of a pre-edge peak

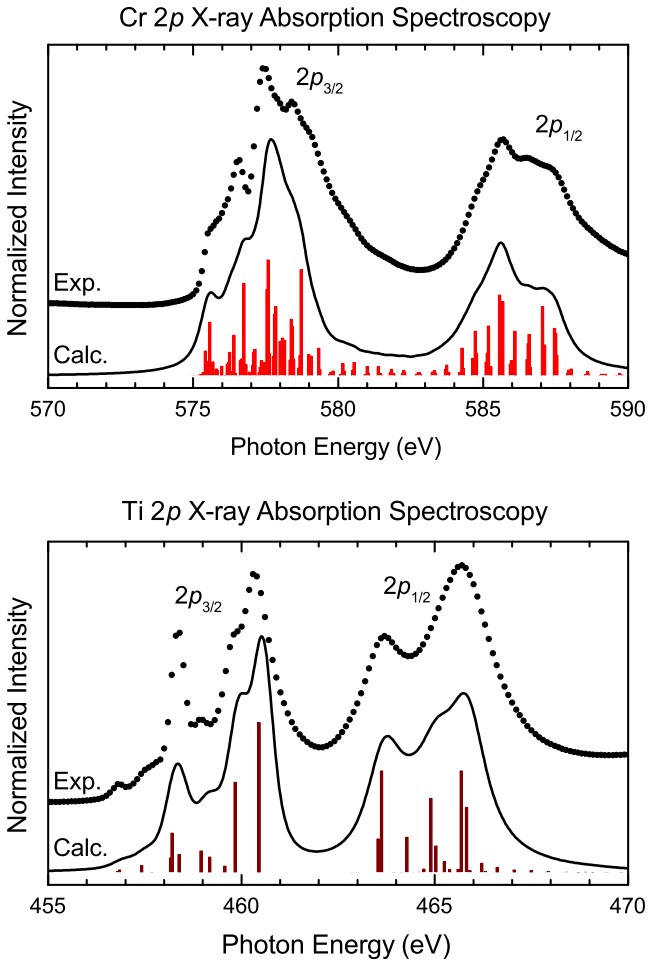

Fig. 4. Experimental Cr (top) and Ti (bottom) $2p$ x-ray absorption spectra of $GdCrTiO_5$ and their calculated spectra via covalent multiplet calculations. The calculated transitions (vertical bars) were broadened (solid line) to simulate the experimental resolution and core hole lifetime.

Table 1
Parameters (in eV) for the charge transfer multiplet calculations of the Cr and Ti $2p$ x-ray absorption spectra.

	10Dq	Dt	Ds	Δ	U	T_σ
Cr^{3+}	1.4	–	–	3.0	6.0	2.8
Ti^{4+}	1.2	0.10	0.18	4.0	4.5	4.0

around 457 eV, a peak around 458.5 eV, a small feature at 459 eV and a shoulder with the major peak centered at 460 eV. The $2p_{1/2}$ region presents similar intensity, but only two major structures appear due to the increase of the lifetime broadening.

Both calculations agree very well with the experiment. The calculated ground state contributions for the Cr^{3+} ion were 49% $3d^3$, 44% $3d^4\underline{L}$, and 7% $3d^5\underline{L}^2$, which gives a mean occupancy of 3.6 electrons. For the Ti^{4+} ions the contributions were 39% $3d^0$, 48% $3d^1\underline{L}$, and 13% $3d^2\underline{L}^2$, corresponding to 0.7 electron in this case.

4.3. O 1s x-ray absorption

The top panel of Fig. 5 presents the comparison between the experimental O $1s$ x-ray absorption spectrum and the unoccupied O $2p$ states from the band structure calculations for $GdCrTiO_5$. The

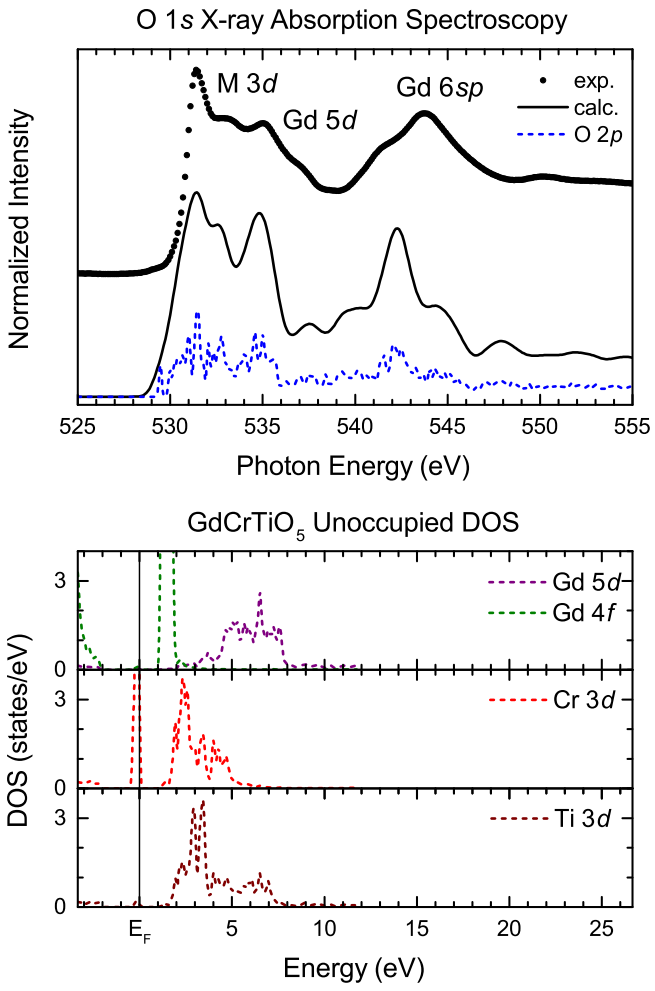

Fig. 5. (Top) Experimental O 1*s* x-ray absorption spectrum of $GdCrTiO_5$ compared to the O 2*p* unoccupied density of states via band structure calculations. The calculated DOS (dashed blue line) was broadened (solid black line) to simulate the experimental resolution. (bottom) Partial Gd 5*d*, Gd 4*f*, Cr 3*d* and Ti 3*d* unoccupied density of states. The solid black line refers to the Fermi energy, and the energy scale was adjusted to match the one in the top panel. (For interpretation of the references to colour in this figure legend, the reader is referred to the web version of this article.)

calculated spectrum was broadened with a Gaussian function with a FWHM of 0.4 eV to account for the experimental resolution and lifetime broadening. The solid and dashed line represent the Gaussian-broadened and the raw O 2*p* unoccupied DOS, respectively.

The experimental spectrum is related to transitions from O 1*s* levels to empty O 2*p* states, which reflects the different metal and rare-earth bands via hybridization. This mixing can be seen in the bottom panel of Fig. 5, which shows the partial DOS from these ions. The vertical line refers to the Fermi energy. The structures between 530 and 533 eV arise from O 2*p* states mixed with Cr 3*d* and Ti 3*d* states. Above 533 eV, the spectrum is dominated mostly by O 2*p* states mixed with Gd 5*d* states and then Gd 6*sp* at higher energies.

The calculated unoccupied O 2*p* DOS agrees remarkably well with the measured data, with small discrepancies in the energy positions above 540 eV. The values of the crystal field splitting 10Dq and intra-atomic exchange interaction J can be estimated from the unoccupied DOS. Inspection of the DOS yielded J ≈ 0.6 eV and 10Dq ≈ 2.0 eV for Cr^{3+}, which is in agreement with the values used in the CTM calculations. The same agreement is found for Ti^{4+}, where 10Dq ≈ 2.4 eV and the intra-atomic exchange is negligible.

4.4. Ground state properties and density of states

Given the good agreement between the O 2*p* DOS and the O 1*s* level x-ray absorption spectrum, we proceed to the analysis of the calculated electronic structure and ground state properties.

A non-magnetic solution could not be obtained, possibly due to the high value of the Gd magnetic moment. Different arrangements of possible magnetic lattices were considered. The AFM solution yielded a total energy around 0.3 eV lower than the FM solutions, which confirms that the ground state is AFM. The inclusion of the spin-orbit effect in the Gd 4*f* levels did not result in any difference in the ground state properties. This result is expected since the $4f^7$ electronic configuration of Gd^{3+} ($^8S_{7/2}$ symmetry) should not present any orbital contribution to the magnetic moment [29]. All results and analysis presented here concern the AFM calculation with the SO effect.

Table 2 presents the total, Gd and Cr magnetic moments obtained from the electronic structure calculations, the present magnetic measurements, as well as from the recently reported Curie-Weiss fitting [19]. The oxygen and titanium ions do not carry magnetic moments. Following Basu et al. [19], non-collinear magnetism between Gd and Cr was assumed, and the calculated total spin was determined as a quadratic sum of individual magnetic moments. The difference between the results may come from the description of the magnetic moments in each method. In the DFT framework, an itinerant approach is assumed, while the Curie-Weiss extrapolation assumes localized magnetic moments.

Fig. 6 presents the band structure calculations for the $GdCrTiO_5$ compound. The density of states shown here comes only from one of the magnetic sublattices. The up and down spin contributions are displayed in the positive and negative y-axis, respectively, and the Fermi energy E_F is denoted by the energy zero (solid black line). The total DOS (not shown) is projected into the Gd 5*d*, Gd 4*f*, Cr 3*d*, Ti 3*d* and O 2*p* orbitals (solid lines), as indicated in the legend. The Gd 4*f* states were cropped so the other contributions could be better visualized. The calculation resulted in an insulating ground state, with a band gap of around 0.83 eV.

In the occupied region (negative energies), the DOS can be split into two main regions: (i) a spin-unpolarized O 2*p* derived band extending from −6.5 eV to −2 eV; (ii) a majority spin Cr 3*d* t_{2g} derived region between −1 eV and E_F, with a small contribution of unpolarized O 2*p* states. The majority spin contribution of Gd 4*f* states appear superimposed in the O 2*p* region, around −4 eV. In the unoccupied region (positive energies), the minority spin Gd 4*f* states dominate the DOS around 1 eV. From 2 to 4 eV the DOS is a mixture of Cr 3*d* and Ti 3*d* with O 2*p* states, while the Gd 5*d* states start to contribute above 4 eV.

In order to clarify the role of the rare-earth in the electronic structure of $GdCrTiO_5$, we performed similar band structure calculations for $NdCrTiO_5$ with the crystal structure reported in Saha et al. [15]. Again, the AFM solution resulted in a lower total energy than the FM case, while a non-magnetic solution was not stabilized.

Table 2
Calculated - with and without spin-orbit coupling (SO) - and measured magnetic moments, in units of μ_B, for the $GdCrTiO_5$ compound.

	Calc.		Expt.	
	no SO	SO	This work	Ref. [19]
Total	9.27	9.29	8.73	8.54
Gd	6.89	6.86	–	–
Cr	2.38	2.43	–	–

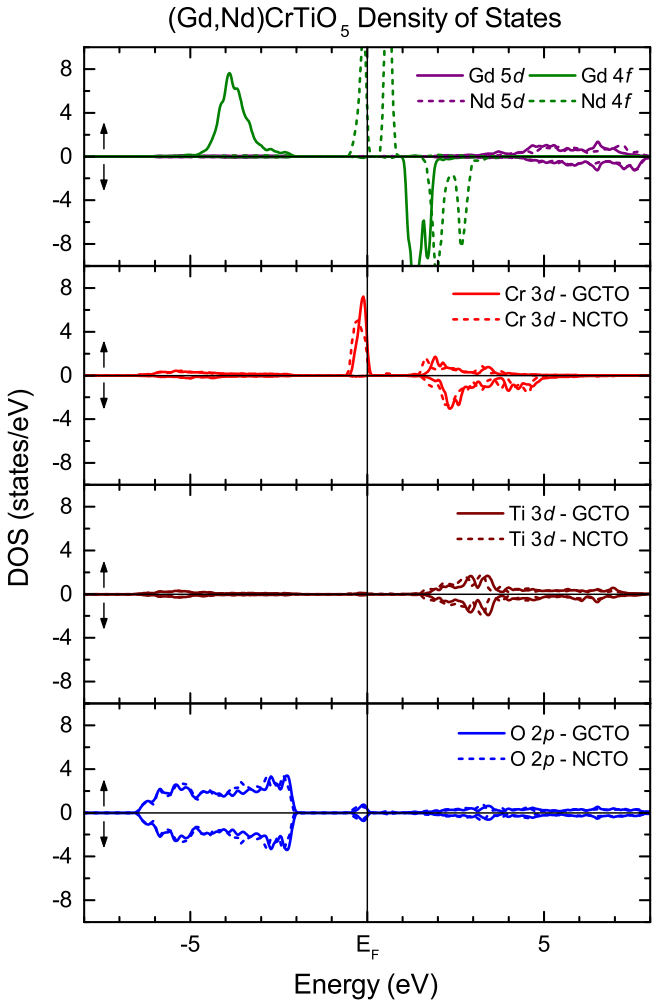

Fig. 6. Calculated partial R 5*d*/4*f*, Cr 3*d*, Ti 3*d*, and O 2*p* densities of states of $GdCrTiO_5$ (GCTO - solid lines) and $NdCrTiO_5$ (NCTO - dashed lines).

Table 3
Calculated - with and without spin-orbit coupling (SO) - and measured magnetic moments, in units of μ_B, for the $NdCrTiO_5$ compound.

	Calc.		Expt.		
	no SO	SO	Ref. [16]	Ref. [30]	Ref. [15]
Total	5.38	5.33	–	5.40	5.73
Nd	3.01	2.97	2.89	–	–
Cr	2.37	2.36	2.95	–	–

The Nd^{3+} ion presents a $4f^3$ electronic configuration, with a spin-only magnetic moment of $3.87\mu_B$. The calculation without the SO interaction resulted in slightly higher magnetic moments, which are summarized and compared with experimental data obtained from Curie-Weiss extrapolation in Table 3.

Fig. 6 also shows the calculated DOS for $NdCrTiO_5$ (dashed lines), decomposed in the partial R 5*d*, R 4*f*, Cr 3*d*, Ti 3*d* and O 2*p* contributions. The electronic structure of the Nd member very much resembles the case of $GdCrTiO_5$, with the only noticeable differences appearing in the R 4*f* partial DOS. The substitution of Nd for Gd extracts four electrons from the system, leaving a partially filled $4f^3$ orbital superimposed to the Cr^{3+} t_{2g} band at −1 eV. The remaining three 4*f* majority states are located at 1 eV, while the minority 4*f* states are pushed towards 2.5 eV.

Table 4
Calculated 4*f* orbital angular momenta in units of $\hbar$ for the rare-earth ion, in each AFM sublattice, in $GdCrTiO_5$ and $NdCrTiO_5$.

R	Sublattice	$\langle L_z\rangle_{up}$	$\langle L_z\rangle_{down}$	$\langle L_z\rangle_{total}$
Gd 4*f*	up	0.00	0.04	0.04
	down	−0.04	0.00	−0.04
Nd 4*f*	up	−1.86	0.02	−1.84
	down	−0.02	1.86	1.84

4.5. Electronic structure and magnetic ordering

Interpretation of the DOS presented in Fig. 6 calls for a reconsideration of the proposed scenario where hybridization of R 4*f*–Cr 3*d* plays a dominant role in the magnetic ordering of the Cr^{3+} network [19]. The electronic structure of the $(CrTiO_5)^{-3}$ anion is virtually the same in both compounds, as well as the calculated magnetic moments of the Cr^{3+} ion. Also, highly hybridized orbitals tend to present similar shapes in the DOS, which does not happen in the calculation presented above. Although the positions of the fully occupied Gd 4*f* majority states (partially filled Nd 4*f* majority states) fall on the same energy region as the O 2*p* band (Cr^{3+} t_{2g} states), the DOS indicate that only a small R 4*f*–Cr 3*d* hybridization may occur, even for the Nd case.

Table 4 shows the calculated 4*f* orbital angular momenta of each rare-earth ion in $GdCrTiO_5$ and $NdCrTiO_5$. The lack of significant orbital angular momenta in the Gd member suggests that, although differences cannot be seen in the density of states or in the magnetic moments, the absence of the SO interaction in this system would decouple spin and orbital degrees of freedom, which would impair the long range magnetic order. Then, even though the Gd ion presents a larger magnetic moment in comparison with Nd, the transition temperatures T_{N1} and T_{N2} found in $GdCrTiO_5$ turn out to be much smaller than those of $NdCrTiO_5$. Thus, conversely to previous results, we propose that spin-orbit coupling may play a key role in the stabilization of the magnetic ordering in $GdCrTiO_5$.

5. Summary and conclusions

We studied the magnetic properties of $GdCrTiO_5$ and a long-range AFM ordering was presented at a low 0.9 K temperature. The electronic structure of this compound was probed with x-ray absorption spectroscopy on the Cr 2*p*, Ti 2*p* and O 1*s* levels. The experimental spectra were interpreted with Charge Transfer Multiplet and Density Functional Theory calculations. The results indicate that spin-orbit interaction, rather than hybridization, may be crucial for the establishment of long range ordering in the $RCrTiO_5$ (R = rare earth) family.

Acknowledgments

This work was supported by Brazil's agencies FAPESP (Grants No. 2013/07296-2 and 2014/19245-6) and CNPq (Grants No. 168255/2014-6, 444712/2014-3, 306006/2105-4, and 153496/2016-9). We acknowledge the PGM beamline staff for technical support and the CNPEM/LNLS to grant beam time under project No. PGM–17732. We thank R. S. Freitas and L. A. S. Moraes for some magnetic and heat capacity data.

References

[1] W. Eerenstein, N.D. Mathur, J.F. Scott, Multiferroic and magnetoelectric materials, Nature 442 (2006) 759–765.
[2] D.N. Astrov, Magnetoelectric effect in chromium oxide, Sov. Phys. JETP 13 (1961) 729–733.
[3] V.J. Folen, G.T. Rado, E.W. Stalder, Anisotropy of the magnetoelectric effect in

Cr_2O_3, Phys. Rev. Lett. 6 (1961) 607–608.
[4] G.T. Rado, Mechanism of the magnetoelectric effect in an antiferromagnet, Phys. Rev. Lett. 6 (1961) 609–610.
[5] G.T. Rado, V.J. Folen, Observation of the magnetically induced magnetoelectric effect and evidence for antiferromagnetic domains, Phys. Rev. Lett. 7 (1961) 310–311.
[6] T. Kimura, Spiral magnets as magnetoelectrics, Annu. Rev. Mater. Res. 37 (2007) 387–413.
[7] S. Kori, T. Okamura, R. Okazaki, I. Terasaki, Y. Yasui, Anomalous magnetic order in the magnetoelectric oxide $NdCrTiO_5$ revealed by impurity effects, Phys. Rev. B 91 (2015) 144403.
[8] S.-W. Cheong, M. Mostovoy, Multiferroics: a magnetic twist for ferroelectricity, Nat. Mater. 6 (2007) 13–20.
[9] J.F. Scott, R. Blinc, Multiferroic magnetoelectric fluorides: why are there so many magnetic ferroelectrics? J. Phys. Condens. Matter 23 (2011) 113202.
[10] R. Ramesh, Ferroelectrics: a new spin on spintronics, Nat. Mater. 9 (2010) 380–381.
[11] A. Inomata, K. Kohn, Pyroelectric effect and possible ferroelectric transition of helimagnetic and, J. Phys. Condens. Matter 8 (1999) 2673.
[12] I. Kagomiya, K. Kohn, T. Uchiyama, Structure and ferroelectricity of RMn_2O_5, Ferroelectrics 280 (2002) 131–143.
[13] N. Hur, S. Park, P.A. Sharma, J.S. Ahn, S. Guha, S.-W. Cheong, Electric polarization reversal and memory in a multiferroic material induced by magnetic fields, Nature 429 (2004) 392–395.
[14] G.R. Blake, L.C. Chapon, P.G. Radaelli, S. Park, N. Hur, S.-W. Cheong, J. Rodríguez-Carvajal, Spin structure and magnetic frustration in multiferroic RMn_2O_5 (R = Tb, Ho, Dy), Phys. Rev. B 71 (2005) 214402.
[15] J. Saha, G. Sharma, S. Patnaik, Evidence for multiferroic characteristics in $NdCrTiO_5$, J. Magn. Magn. Mater. 360 (2014) 34–37.
[16] G. Buisson, Etude par rayons X et neutrons de la serie isomorphe $ATiTO_5$ (A = Cr, Mn, Fe, T = Terres Rares), J. Phys. Chem. Solids 31 (1970) 1171–1183.
[17] X.L. Qian, Y.F. Fang, J. Kang, S.X. Cao, J.C. Zhang, Influence of Sm^{3+} substitution on the multiferroic effect in $NdCrTiO_5$, Phys. B Condens. Matter 495 (2016) 1–3.
[18] J. Hwang, E.S. Choi, H.D. Zhou, J. Lu, P. Schlottmann, Magnetoelectric effect in $NdCrTiO_5$, Phys. Rev. B 85 (2012) 024415.
[19] T. Basu, K. Singh, S. Gohil, S. Ghosh, E.V. Sampathkumaran, Implications of magnetic and magnetodielectric behavior of $GdCrTiO_5$, J. Appl. Phys. 118 (2015) 234103.
[20] H. Jang, B.Y. Kang, B.K. Cho, M. Hashimoto, D. Lu, C.A. Burns, C.C. Kao, J.S. Lee, Observation of orbital order in the half-filled 4*f* Gd compound, Phys. Rev. Lett. 117 (2016) 216404.
[21] E. Stavitski, F.M.F. de Groot, The CTM4XAS program for EELS and XAS spectral shape analysis of transition metal L edges, Micron 41 (2010) 687–694.
[22] R. Cowan, The Theory of Atomic Structure and Spectra, Los Alamos Series in Basic and Applied Sciences, University of California Press, 1981.
[23] A.E. Bocquet, T. Mizokawa, T. Saitoh, H. Namatame, A. Fujimori, Electronic structure of 3d-transition-metal compounds by analysis of the 2p core-level photoemission spectra, Phys. Rev. B 46 (1992) 3771–3784.
[24] M. Imada, A. Fujimori, Y. Tokura, Metal-insulator transitions, Rev. Mod. Phys. 70 (1998) 1039–1263.
[25] M.O. Krause, J.H. Oliver, Natural widths of atomic K and L levels, Kα X-ray lines and several KLL Auger lines, J. Phys. Chem. Ref. Data 8 (1979) 329–338.
[26] P. Blaha, K. Schwarz, G. Madsen, D. Kvasnicka, J. Luitz, WIEN2k, an Augmented Plane Wave + Local Orbitals Program for Calculating Crystal Properties, Vienna, 2001.
[27] J.P. Perdew, A. Ruzsinszky, G.I. Csonka, O.A. Vydrov, G.E. Scuseria, L.A. Constantin, X. Zhou, K. Burke, Restoring the density-gradient expansion for exchange in solids and surfaces, Phys. Rev. Lett. 100 (2008) 136406.
[28] B.H. Toby, EXPGUI, a graphical user interface for GSAS, J. Appl. Crystallogr. 34 (2001) 210–213.
[29] B.T. Thole, P. Carra, F. Sette, G. van der Laan, X-ray circular dichroism as a probe of orbital magnetization, Phys. Rev. Lett. 68 (1992) 1943–1946.
[30] M. Greenblatt, R.M. Hornreich, B. Sharon, Magnetoelectric compounds with two sets of magnetic sublattices: $UCrO_4$ and $NdCrTiO_5$, J. Solid State Chem. 10 (1974) 371–376.